Biochemical and Biophysical Research Communications 430 (2013) 1272–1276

Contents lists available at SciVerse ScienceDirect

Biochemical and Biophysical Research Communications

journal homepage: www.elsevier.com/locate/ybbrc

Distinct interactions of Na^+ and Ca^{2+} ions with the selectivity filter of the bacterial sodium channel Na_VAb

Song Ke, Eva-Maria Zangerl, Anna Stary-Weinzinger *

Department of Pharmacology and Toxicology, University of Vienna, Althanstrasse 14, UZA 2, A-1090 Vienna, Austria

ARTICLE INFO

Article history:
Received 5 December 2012
Available online 19 December 2012

Keywords:
Bacterial sodium channel
Ca^{2+} selectivity
Free energy profile
Ion binding sites
Molecular dynamics simulation

ABSTRACT

Rapid and selective ion transport is essential for the generation and regulation of electrical signaling pathways in living organisms. In this study, we use molecular dynamics simulations and free energy calculations to investigate how the bacterial sodium channel Na_VAb (*Arcobacter butzleri*) differentiates between Na^+ and Ca^{2+} ions. Multiple nanosecond molecular dynamics simulations revealed distinct binding patterns for these two cations in the selectivity filter and suggested a high affinity calcium binding site formed by backbone atoms of residues Leu-176 and Thr-175 (S_{CEN}) in the sodium channel selectivity filter.

1. Introduction

Na^+ flux is vital for initiating action potentials in the membranes of most electrically excitable cells [1]. Recent homotetrameric crystal structures of bacterial Na_V channels [2–5] provide new possibilities for investigating the molecular basis of ion selectivity and transport in these channels. The mechanisms of how these channels discriminate between different ion types are poorly understood. Recent molecular dynamics investigations [6,7] provide insights into Na^+ versus K^+ selectivity; however Ca^{2+} discrimination was not analyzed in atomistic detail so far. In this study, we investigate how bacterial sodium channels discriminate between Na^+ and Ca^{2+}, a process essential for biological function.

Na_V channels are composed of four membrane spanning subunits, containing six helices per subunit. The pore module consists of helices S5, P1 segments, a selectivity filter (SF) region, P2 segments and S6 helices, lining the inner pore cavity. Remarkably, the SF of many bacterial sodium channels contains four highly conserved glutamates (EEEE locus), which is more reminiscent of calcium channels than mammalian sodium channels [8–11]. Despite this high sequence similarity, bacterial Na_V channels distinguish between sodium and calcium ions with permeability ratios P_{Ca}/P_{Na} of 0.08–0.15 [12,13]. The three dimensional architecture of this motif is revealed by X-ray structures of bacterial Na_V channels from three different species [2–5]. How these unusual sodium channels discriminate between different ion types and how ions permeate the pore are not well understood yet.

In this study, we performed molecular dynamics (MD) simulations and single ion potential of mean force (PMF) calculations to investigate Ca^{2+} interactions with the bacterial sodium channel Na_VAb.

2. Materials and methods

2.1. Molecular dynamics simulations

MD simulations were performed with Gromacs version 4.5.4 [14]. The coordinates of Na_VAb (PDB Entry: 3RVY; resolution: 2.7 Å) with a closed pore gate were used in all simulations [2]. Cysteine residues at position 217 were mutated back to isoleucine to obtain the wild-type structure of Na_VAb, and all charged residues were treated keeping their charge states at physiological pH 7.4. Simulations were carried out with the AMBER99sb [15] all atom force field in dioleoylphospathidylcholine (DOPC) lipids [16] with the TIP3P water model [17].

All covalent bonds were constrained using the LINCS algorithm [18], allowing for an integration time step of 2 fs. A 10 Å cutoff was adopted for calculating short-range electrostatic interactions and the Particle Mesh Ewald [19] summation was used for calculating long-range electrostatic interactions. The corrected Lennard-Jones parameters for the amber forcefield [20] were implemented in this

Abbreviations: Na_VAb, bacterial sodium channel (*Arcobacter butzleri*); Na_VRh, bacterial sodium channel (*Rickettsiales* sp. *HIMB114*); MD simulation, molecular dynamics simulation; PMF, potential of mean force; SF, selectivity filter; DOPC, dioleoylphospathidylcholine; PDB, protein data bank; RMSD, root-mean-square deviation.

* Corresponding author. Fax: +43 1 4277 9553.
E-mail addresses: song.ke@univie.ac.at (S. Ke), a0509032@unet.univie.ac.at (E.-M. Zangerl), anna.stary@univie.ac.at (A. Stary-Weinzinger).

0006-291X/$ - see front matter © 2012 Elsevier Inc. All rights reserved.
http://dx.doi.org/10.1016/j.bbrc.2012.12.055

study and the vdW interactions were calculated with a cutoff of 10 Å. The Nose–Hoover thermostat [21,22] and the semi-isotropic Parrinello-Rahman barostat algorithm [23] was used to maintain simulation temperature and pressure constantly at 310 K and 1 bar, respectively. Prior to MD simulations, 3000 conjugate gradient energy-minimization steps were performed, followed by 5 ns equilibration in order to fully solvate mobile water and lipids around a protein restrained with a force constant of 1000 kJ/mol/nm^2 on all heavy atoms.

2.2. PMF

One ion PMF calculations were performed by umbrella sampling [24]. Prior to this simulation, a test ion was pulled with a force constant of 2090 kJ/mol/nm^2 (5 kcal/mol/Å^2) along the filter, from a heavily restrained (force constant: 10,000 kJ/mol/nm^2) reference ion (placed ~15 Å away on top of the extracellular side of the filter) [25]. This procedure resulted in 20 windows to explore the ion conductance route along the filter (total length ~10 Å, as shown in Fig 1B inset) at 0.5 Å intervals. The test ion was initially held fixed for a 100 ps equilibration, followed by a 2 ns PMF simulations with the first 0.5 ns removed for equilibration [7]. In each umbrella sampling simulation, the probing ion was restrained harmonically with a force constant of 4180 kJ/mol/nm^2 (10 kcal/mol/Å^2) along the *z*-axis. A 4.18 kJ/mol/nm^2 (0.01 kcal/mol/Å^2) force constant was exerted on the Cα atoms of the protein as a center of mass restraint during simulations, except for the SF residues (residues 174–183) [7]. The free energy profile was calculated with the g_wham tool implemented in Gromacs. Error analysis was performed calculating 200 bootstrap iterations [26].

3. Results and discussions

Two 100 ns MD simulations with 100 mM NaCl and 100 mM $CaCl_2$ concentrations each were performed. A third simulation with either NaCl or $CaCl_2$ was extended to 150 ns for analysis. To get further insight into the different behavior of Na^+ and Ca^{2+} ions in the

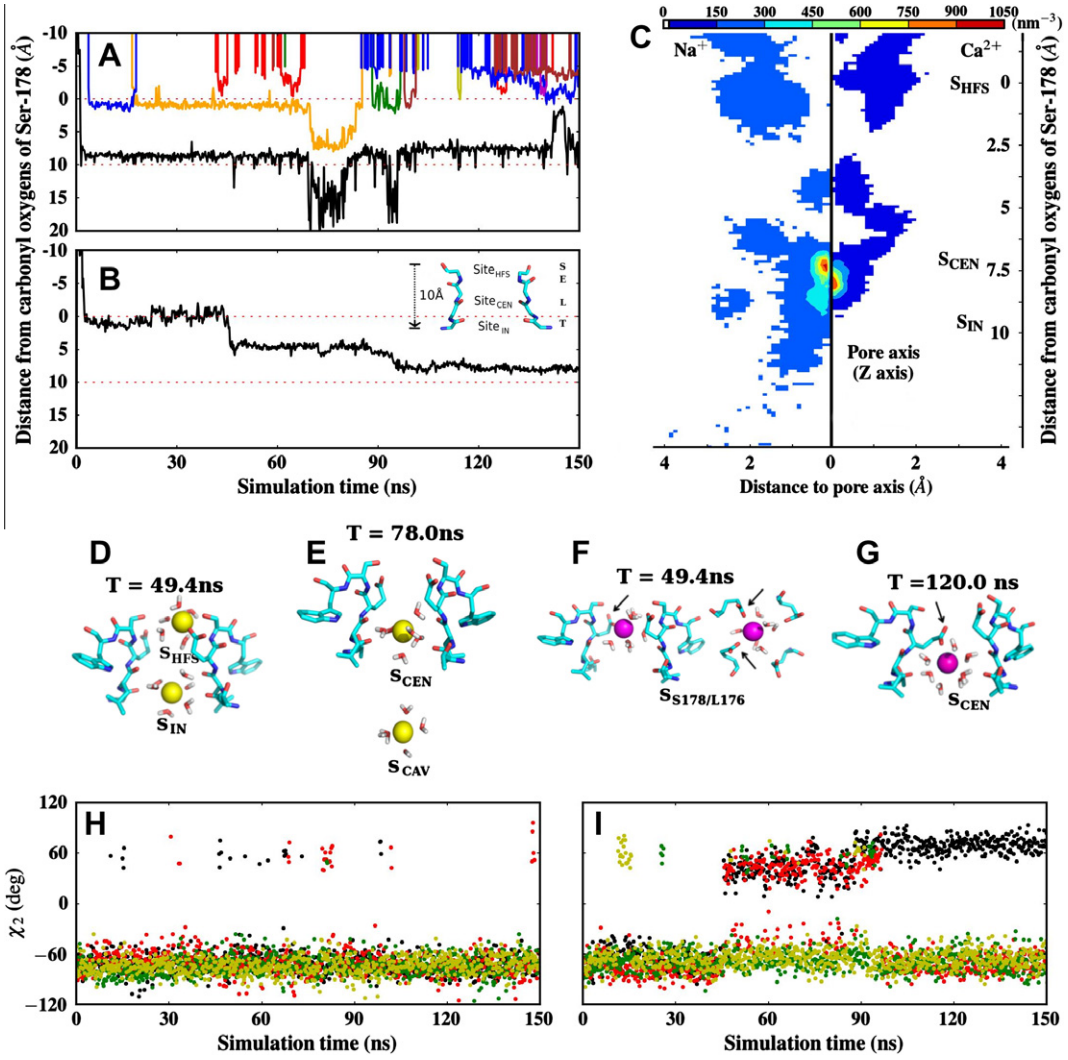

Fig. 1. Na^+ and Ca^{2+} binding patterns inside the Na_VAb SF. (A) Binding patterns of Na^+ ions as a function of time (snapshots from every 200 ps), the *y*-axis depicts the distances along the pore axis (*z*-axis) to the entrance of the SF (carbonyl oxygen atoms of Ser-178) from the extracellular solution; two red dotted lines highlight the entrance and the exit of the SF (backbone nitrogen atom of Thr-175); the inset shows the binding sites suggested by Payandeh et al. [2]. (B) Binding pattern of Ca^{2+} as a function of time (snapshots from every 200 ps). (C) Ion distribution maps of Na^+ s and Ca^{2+} inside the selectivity filter (snapshots from every 10 ps). (D) Filter snapshot of Na^+ ions at 49.4 ns; the Na^+ ions are shown as yellow spheres. (E) Filter snapshot depicting Na^+ ion positions at 78.0 ns. (F) Ca^{2+} snapshots (side and top view) taken at 49.4 ns, with Ca^{2+} shown in magenta; the black arrows indicate the side chain conformational change of Glu-177. (G) Filter snapshot taken at 120.0 ns. (H) Analysis of the χ_2 angle of Glu-177 as of function of time for NaCl (snapshots from every 200 ps); Side chains of the different subunits are colored black, red, yellow and green respectively. (I) Changes of Glu-177 χ_2 angles induced by Ca^{2+} binding as of function of time (snapshots from every 200 ps).

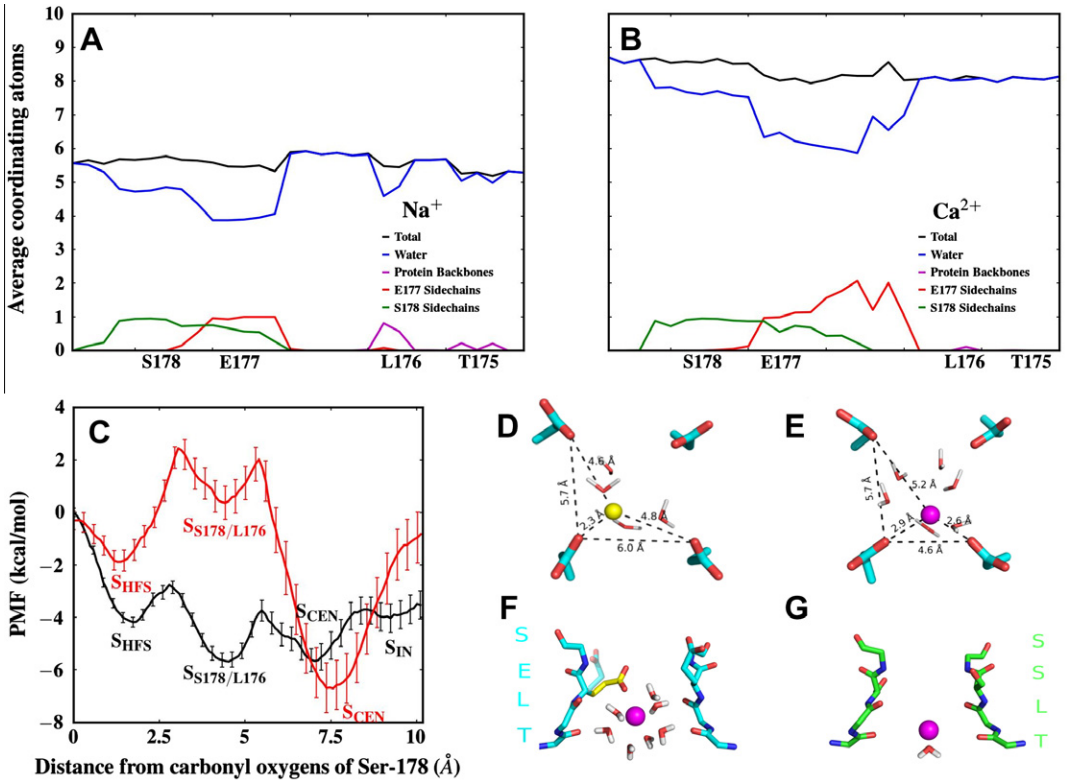

Fig. 2. Ion coordination and PMF comparison between Na^+ and Ca^{2+}. Oxygen atoms closer than 2.8 Å (Na^+) or 3.0 Å (Ca^{2+}) were considered coordinating atoms [35]. (A) Average oxygen coordination numbers for Na^+: the total coordination number is depicted in black; water oxygens are depicted as blue lines, protein backbone oxygens are shown in magenta, Glu-177 side chain are colored red and Ser-178 side chain are shown as green lines (windows of all umbrella-sampling runs were taken for analysis, taking snapshots every 15 ps). (B) Average coordination oxygen atoms numbers for Ca^{2+} colored similar as in Fig. 2A. (C) Single-ion free energy profile of Na^+ (black) and Ca^{2+} (red); The energy minima of Na^+ in site S_{HFS}, $S_{S178/L176}$, S_{CEN} and S_{IN} are shown (annotations taken from Payandeh et al. [2]); The energy minima for Ca^{2+} in sites S_{HFS}, $S_{S178/L176}$, and S_{CEN} are colored in red. (D) Snapshot capturing the transition of Na^+ from site S_{HFS} to site $S_{S178/L176}$ with distances between Na^+ (yellow sphere) and adjacent carboxyl oxygens from Glu-177 and Glu-177- Glu-177 distances labeled. (E) Snapshot capturing the transition barrier of Ca^{2+} (magenta sphere) from site S_{HFS} to site $S_{S178/L176}$. (F) Snapshot of Ca^{2+} at site $S_{CEN;}$ the conformational change of Glu-177 side chain is shown in yellow; the cyan shadow indicates the original conformation of this side chain. (G) The crystal structure of Na_VRh revealing a similar Ca^{2+} binding site in the SF [4].

SF, one-ion free energy profiles were calculated along the filter, see Fig. 1 B inset. The binding sites are annotated S_{HFS}, S_{IN} and S_{CEN} in line with Payandeh et al. [2].

3.1. Na^+ and Ca^{2+} binding patterns in the SF

In all six MD simulations the RMSD of the backbone atoms of the SF was below 1.0 Å, indicating stability of the filter. Fig. 1A and B reveal differences in the dynamics of Na^+ and Ca^{2+} binding to the SF of Na_VAb. In agreement with recent MD simulations [27,28], sodium ions can move into the SF from the extracellular bulk water within 5 ns (Fig. 1A). Two Na^+ ions spontaneously accommodated the two favorable sites S_{HFS} and S_{IN} in a hydrated manner (Fig. 1A and D) [6,7]. Occasionally, a sodium ion was observed to spontaneously move into the cavity and back up to site S_{IN} of the SF (Fig. 1A and E). Since the intracellular gate of this crystal structure is closed, no ion conducting event was observed. Similar to sodium, a calcium ion entered the SF from the extracellular bulk water within 5 ns (Fig 1B). However, the Ca^{2+} ion occupied site S_{HFS} for ~40 ns. After 45 ns, Ca^{2+} migrated into a new site formed by backbone nitrogen atoms of residues Ser-178 and Leu-176 (site $S_{S178/L176}$) above site S_{CEN} (Fig. 1B and F). After ~95 ns, calcium moved into site S_{CEN} where it remained for the rest of the simulation (Fig. 1B, C and G). In contrast to simulations with NaCl, in all three simulations with $CaCl_2$, only one Ca^{2+} ion was found to bind to the SF.

3.2. SF dynamics – influence of ion type

Analysis of the trajectory revealed that, in contrast to Na^+ where the filter remained rigid, Ca^{2+} ions induced changes of the Glu-177 side chain (see Fig. 1H and I). After ~45 ns, the χ_2 angles of two adjacent Glu-177 side chains changed from −70° to 45°. These changes facilitate collective Ca^{2+} coordination from two neighboring Glu side chains at site $S_{S178/L176}$ (Fig. 1F and Fig. 2B). After this intermediate state (started from 90 ns), one of the side chains flipped back to its native conformation as observed in the crystal structure, whereas the conformation of the second glutamate changed even further to ~70° (Fig. 1I) when coordinating a Ca^{2+} ion at site S_{CEN} (Fig. 1G). These filter changes enabled more favorable electrostatic interactions with Ca^{2+}.

3.3. Free energy differences

To investigate possible differences in free energy profiles of these two ion species, we performed PMF calculations (Fig. 2C). Since only one calcium ion was observed to occupy the SF in repeated simulations, we calculated one-ion PMFs. The free energy profile of sodium shows four local minima: at site S_{HFS}, site $S_{S178/L176}$, site S_{CEN}, and site S_{IN}. These calculations revealed that Na^+ has no energy barrier higher than 2.1 kcal/mol, suggesting that sodium ions can easily pass the filter. These values are in close agreement with previous studies [6,7,28]. PMF calculations with calcium revealed an energy barrier of approximately ~4.3 kcal/mol

compared to ~1.4 kcal/mol for Na^+. This relatively high barrier is located between sites S_{HFS} and $S_{S178/L176}$ (Fig. 2C), indicating that Ca^{2+} discrimination might occur in this region of the SF. Further analyses of the structural snapshots suggested that this region of the SF does not provide an ideal geometry for calcium ions. Distance measurements between coordinating glutamate oxygens and Ca^{2+}, revealed a less favorable, asymmetric coordination pattern compared to sodium (See Fig. 2D and E). A similar mechanism, albeit at a slightly different site in the SF was proposed by Corry and Thomas for Na^+ versus K^+ discrimination [7]. This energy barrier might be part of the reason why Ca^{2+} movement to site S_{CEN} (Fig. 1B) was rather slow (after ~90 ns versus after ~5 ns for Na^+). The lowest energy well for Ca^{2+} is approximately at site S_{CEN}. Further, PMF calculations revealed that there is a large energy barrier (~5 kcal/mol) for calcium ions after site S_{CEN}, which might prevent movement into the cavity. Remarkably, the high affinity binding site at site S_{CEN} (Fig. 2F) agrees well with the X-ray data by Zhang et al. [4] on the related Na_VRh channel, showing a Ca^{2+} ion bound at site L179/T178 (Fig. 2G).

3.4. Comparison of Na^+ and Ca^{2+} ion coordination

Next, we compared ion solvation patterns for Na^+ and Ca^{2+} in the Na_VAb SF. The nature of the atoms coordinating either a single Na^+ ion or a single Ca^{2+} ion at different positions along the permeation pore are shown in Fig. 2A and B. In accordance with previous simulations on Na^+ permeation, Na^+ ions can bind inside the SF with the entire or part of the inner hydration shell intact [6,7,27,28]. In site S_{HFS}, two of the water molecules from the hydration shell were substituted by side chain oxygen atoms of Glu-177 and Ser-178; at site S_{CEN}, one of the coordinating water molecules was replaced by a carbonyl oxygen atom of Leu-176 (Fig. 2A).

Hydration patterns for Ca^{2+} are shown in Fig 2B. In contrast to sodium, where only one glutamate participates in ion coordination, the conformational changes of the Glu-177 side chains allowed Ca^{2+} coordination with two glutamate side chain oxygen atoms. The pivotal role of the flipped Glu-177 side chain(s) is shown in Fig. 1F, G and I and Fig. 2B. Further, these side chain changes rendered the coordination by Leu-176 backbone oxygen atoms less likely. As a result, the Ca^{2+} distribution was restricted to the center of the pore axis (Fig. 1C, right).

Summarizing, our studies revealed clear differences for Na^+ versus Ca^{2+} behavior in the Na_VAb SF. MD simulations highlight the importance of electrostatic interactions to discriminate between Na^+ and Ca^{2+} in bacterial sodium channels. This is consistent with previous theoretical studies [29–34] of Ca^{2+} and Na^+ channels, which suggested that ion discrimination is primarily governed by electrostatic interactions in the EEEE locus. Interestingly, the association times for Ca^{2+} were rather slower compared to Na^+, which might be explained by a lack of a "loose" knock-on mechanism, shown to be important for Na^+ conductance by recent MD studies [6,7]. In none of our three $CaCl_2$ simulations more than one Ca^{2+} entered the SF. It should be stressed that longer simulation times might be needed to further validate this observation. Future investigations combining NaCl and $CaCl_2$ will be necessary to reveal the role of multi-ion interactions (e.g. Na^+–Ca^{2+} interactions) within the SF.

Acknowledgments

We thank Tobias Linder for helpful discussions and critical reading of the manuscript. This work was supported by The Austrian Science Fund (Grant W1232). The computational results presented have been achieved using the Vienna Scientific Cluster (VSC).

References

[1] W.A. Catterall, From ionic currents to molecular review mechanisms: the structure and function of voltage-gated sodium channels, Neuron 26 (2000) 13–25.
[2] J. Payandeh, T. Scheuer, N. Zheng, W.A. Catterall, The crystal structure of a voltage-gated sodium channel, Nature 475 (2011) 353–358.
[3] J. Payandeh, T.M.G. El-Din, T. Scheuer, N. Zheng, W.A. Catterall, Crystal structure of a voltage-gated sodium channel in two potentially inactivated states, Nature 486 (2012) 135–139.
[4] X. Zhang, W. Ren, P. DeCaen, C. Yan, X. Tao, L. Tang, et al., Crystal structure of an orthologue of the NaChBac voltage-gated sodium channel, Nature 486 (2012) 130–134.
[5] E.C. McCusker, C. Bagnéris, C.E. Naylor, A.R. Cole, N. D'Avanzo, C.G. Nichols, et al., Structure of a bacterial voltage-gated sodium channel pore reveals mechanisms of opening and closing, Nat. Commun. 3 (2012) 1102.
[6] S. Furini, C. Domene, On conduction in a bacterial sodium channel, PLoS Comput. Biol. 8 (2012) e1002476.
[7] B. Corry, M. Thomas, Mechanism of ion permeation and selectivity in a voltage gated sodium channel, J. Am. Chem. Soc. 134 (2011) 1840–1846.
[8] W.A. Sather, E.W. McCleskey, Permeation and selectivity in calcium channels, Annu. Rev. Physiol. 65 (2003) 133–159.
[9] R. Dejian, Sodium leak channels in neuronal excitability and rhythmic behaviors, Neuron 72 (2011) 899–911.
[10] J. Yang, P.T. Elllnor, W.A. Sather, J.I.F. Zhang, R.W. Tsien, Molecular determinants of Ca^{2+} selectivity and ion permeation in L-type Ca^{2+} channels, Nature 366 (1993) 158–161.
[11] S.H. Heinemann, H. Terlau, W. Stühmer, K. Imoto, S. Numa, Calcium channel characteristics conferred on the sodium channel by single mutations, Nature 356 (1992) 441–443.
[12] L. Yue, B. Navarro, D. Ren, A. Ramos, D.E. Clapham, The cation selectivity filter of the bacterial sodium channel, NaChBac, J. Gen. Physiol. 120 (2002) 845–853.
[13] D. Shaya, M. Kreir, R.A. Robbins, S. Wong, J. Hammon, A. Brüggemann, et al., Voltage-gated sodium channel (Na_V) protein dissection creates a set of functional pore-only proteins, Proc. Nat. Acad. Sci. 108 (2011) 12313.
[14] B. Hess, C. Kutzner, D. Van Der Spoel, E. Lindahl, GROMACS 4: algorithms for highly efficient, load-balanced, and scalable molecular simulation, J. Chem. Theory Comput. 4 (2008) 435–447.
[15] V. Hornak, R. Abel, A. Okur, B. Strockbine, A. Roitberg, C. Simmerling, Comparison of multiple Amber force fields and development of improved protein backbone parameters, Proteins 65 (2006) 712–725.
[16] S.W.I. Siu, R. Vácha, P. Jungwirth, R.A. Böckmann, Biomolecular simulations of membranes: physical properties from different force fields, J. Chem. Phys. 128 (2008) 125103.
[17] W.L. Jorgensen, J. Chandrasekhar, J.D. Madura, R.W. Impey, M.L. Klein, Comparison of simple potential functions for simulating liquid water, J. Chem. Phys. 79 (1983) 926–935.
[18] B. Hess, H. Bekker, H.J.C. Berendsen, J.G.E.M. Fraaije, LINCS: a linear constraint solver for molecular simulations, J. Comput. Chem. 18 (1997) 1463–1472.
[19] T. Darden, D. York, L. Pedersen, Particle Mesh Ewald: an N log (N) method for Ewald sums in large systems, J. Chem. Phys. 98 (1993). 10089-10089.
[20] I.S. Joung, T.E. Cheatham III, Determination of alkali and halide monovalent ion parameters for use in explicitly solvated biomolecular simulations, J. Phys. Chem. B 112 (2008) 9020–9041.
[21] S. Nose, A unified formulation of the constant temperature molecular-dynamics methods, J. Chem. Phys. 81 (1984) 511–519.
[22] W.G. Hoover, Canonical dynamics: equilibrium phase-space distributions, Phys. Rev. A 31 (1985) 1695–1697.
[23] R. Martoňák, A. Laio, M. Parrinello, Predicting crystal structures: the Parrinello-Rahman method revisited, Phys. Rev. Lett. 90 (2003) 75503.
[24] G.M. Torrie, J.P. Valleau, Monte Carlo free energy estimates using non-Boltzmann sampling: application to the sub-critical Lennard-Jones fluid, Chem. Phys. Lett. 28 (1974) 578–581.
[25] J.A. Lemkul, D.R. Bevan, Assessing the stability of Alzheimer's amyloid protofibrils using molecular dynamics, J. Phys. Chem. B 114 (2010) 1652–1660.
[26] J.S. Hub, B.L. de Groot, D. van der Spoel, G_wham—a free weighted histogram analysis implementation including robust error and autocorrelation estimates, J. Chem. Theory Comput. 6 (2010) 3713–3720.
[27] V. Carnevale, W. Treptow, M.L. Klein, Sodium ion binding sites and hydration in the lumen of a bacterial ion channel from molecular dynamics simulations, J. Phys. Chem. Lett. 2 (2011) 2504–2508.
[28] H. Qiu, R. Shen, W. Guo, Ion solvation and structural stability in a sodium channel investigated by molecular dynamics calculations, Biochim. Biophys. Acta (BBA) – Biomembr. 2012 (1818) 2529–2535.
[29] D. Boda, D.D. Busath, D. Henderson, S. Sokolowski, Monte Carlo simulations of the mechanism for channel selectivity: the competition between volume exclusion and charge neutrality, J. Phys. Chem. B 104 (2000) 8903–8910.
[30] D. Boda, D.D. Busath, B. Eisenberg, D. Henderson, W. Nonner, Monte Carlo simulations of ion selectivity in a biological Na channel: charge–space competition, Phys. Chem. Chem. Phys. 4 (2002) 5154–5160.
[31] D. Boda, T. Varga, D. Henderson, D.D. Busath, W. Nonner, D. Gillespie, et al., Monte Carlo simulation study of a system with a dielectric

boundary: application to calcium channel selectivity, Mol. Simul. 30 (2004) 89–96.
[32] B. Corry, S.H. Chung, Mechanisms of valence selectivity in biological ion channels, Cell. Mol. Life Sci. 63 (2006) 301–315.
[33] T. Dudev, C. Lim, Why voltage-gated Ca^{2+} and bacterial Na^{+} channels with the same EEEE motif in their selectivity filters confer opposite metal selectivity, Phys. Chem. Chem. Phys. 14 (2012) 12451–12456.
[34] T. Dudev, C. Lim, Competition among Ca^{2+}, Mg^{2+}, and Na^{+} for model ion channel selectivity filters: determinants of ion selectivity, J. Phys. Chem. B 116 (2012) 10703–10714.
[35] S. Koneshan, J.C. Rasaiah, R.M. Lynden-Bell, S.H. Lee, Solvent structure, dynamics, and ion mobility in aqueous solutions at 25 °C, J. Phys. Chem. B 102 (1998) 4193–4204.